

(HUANJING KEXUE)

# ENVIRONMENTAL SCIENCE

第38卷 第10期

Vol.38 No.10

2017

中国科学院生态环境研究中心 主办

科学出版社出版



## ENVIRONMENTAL SCIENCE

第38卷 第10期 2017年10月15日

## 目 次

中国城市热岛时空特征及其影响因子的分析
□□□□□□□□□□□□□□□□□□□□□□□□□□□□□□□□□□□□
□□□□□□□□□□□□□□□□□□□□□□□□□□□□□□□□□□□□
岩溶关键带微量元素运移的时空变化:以豫西鸡冠洞为例 ··· 梁沙,杨琰,张娜,孙喆,张萍,田宁,凌新有,任小敏(4130) 龟石水库夏季富营养化状况与蓝藻水华暴发特征 ····································
阿哈水库叶绿素 a 时空分布特征及其与藻类、环境因子的关系 罗宜富,李磊,李秋华,焦树林,李红梅,陈峰峰(4151) 天目湖沙河水库浮游植物群落结构的时空异质性
程海沉积物重金属时空变化及人为污染与潜在生态风险 ······· 于真真, 刘恩峰, 张恩楼, 林琪, 沈吉, 王荣, 李艳玲(4169)自然降雨条件下红壤坡地磷素随径流垂向分层输出特征 ··········· 左继超, 郑海金, 奚同行, 王凌云, 聂小飞, 刘昭(4178)邻苯二甲酸酯在三峡库区消落带非淹水期土壤中污染特征及健康风险 ············ 杨婷, 何明靖, 杨志豪, 魏世强(4187)滦河干流水体多环芳烃与有机氯农药季节性分布、组成及源解析 ····································
董政, 马玉龙, 李珺琪, 袁浩东, 金军, 王英(4212) 道路灰尘中有机磷阻燃剂污染特征及人体暴露 ········李静, 王俊霞, 许婉婷, 尚荣双, 顾海东, 温耀进, 张丽君(4220) 居民经手口途径摄入含 PAHs 颗粒物的致癌风险评价 ····································
一個大學學學學學學學學學學學學學學學學學學學學學學學學學學學學學學學學學學學學
四段式曝气对好氧颗粒污泥脱氮性能的影响
基于总量及形态的土壤重金属生态风险评价对比:以龙岩市适中镇为例
猪粪堆肥过程中金霉素去除及重金属形态变化
機生物多样性对土壤碳代谢特征的影响 吴蔓莉,陈凯丽,叶茜琼,祁燕云,徐会宁,王卓,薛鹏飞,朱常琳(4412) 微生物多样性对土壤碳代谢特征的影响 安小麦田 O3 气孔与非气孔沉降及风险评估 徐静馨,郑有飞,赵辉,储仲芳,黄积庆,袁月(4427) 中国西南酸雨区降水化学特征研究进展 周晓得,徐志方,刘文景,武瑶,赵童,蒋浩(4438) 《环境科学》征稿简则(4261) 《环境科学》征订启事(4270) 信息(4186, 4404, 4446)

## 中国城市热岛时空特征及其影响因子的分析

曹畅1,2,李旭辉1,2,张弥1,2,刘寿东1,2,徐家平1,2

(1. 南京信息工程大学大气环境中心,南京 210044; 2. 南京信息工程大学江苏省大气环境与装备技术协同创新中心,南京 210044)

摘要:全球气候变暖背景下,城市热岛效应会加重城市地区的热胁迫,对人类健康和生存发展提出严峻挑战.近年来我国雾-霾污染情况严重,但雾-霾对城市热岛影响的认识仍较匮乏.本研究基于 MODIS 遥感卫星地表温度数据,明确了我国 2003~2013年白天、夜间以及四季城市热岛的空间变化,并从生物物理学和生物化学角度定量分析其控制机制.结果表明,影响我国白天城市热岛强度的主要因素为人口、农田灌溉和植被活动.纬度、降水量、反照率以及气溶胶浓度是夜间城市热岛强度的主控因子.从对比城乡粗糙度、反照率等生物物理学属性的角度,揭示了乡村背景环境对城市热岛分析的重要影响.结果表明,雾-霾治理可以缓解我国夜间城市热岛现象和热胁迫,有利于缓解区域甚至全球气候变化.

关键词:城市热岛;气候区;气溶胶;地表温度;遥感

中图分类号: X16 文献标识码: A 文章编号: 0250-3301(2017)10-3987-11 DOI: 10.13227/j. hjkx. 201702127

# Correlation Analysis of the Urban Heat Island Effect and Its Impact Factors in China

CAO Chang<sup>1,2</sup>, LI Xu-hui<sup>1,2</sup>, ZHANG Mi<sup>1,2</sup>, LIU Shou-dong<sup>1,2</sup>, XU Jia-ping<sup>1,2</sup>

(1. Yale-NUIST Center on Atmospheric Environment, Nanjing University of Information Science and Technology, Nanjing 210044, China; 2. Jiangsu Collaborative Innovation Center of Atmospheric Environment and Equipment Technology (CICAEET), Nanjing University of Information Science and Technology, Nanjing 210044, China)

Abstract: Urban heat islands (UHIs), which are urban areas with higher surface or air temperatures than surrounding rural areas, can further enhance the heat stress already exacerbated by global warming. This poses great challenges to human health and sustainable development. China has been burdened with heavy air pollution in recent years, and the effect of haze pollution on UHIs is still far less well understood. This study investigated the spatial variations of daytime, nighttime, and seasonal surface UHI effects in China during 2003-2013, based on MODIS land surface temperature data, and analyzed the correlations between the UHI effect and its impact factors from both biophysical and biochemical perspectives. Our results show that MODIS-derived annual nighttime UHI effect (3.4 K  $\pm$  0.2 K, mean ±1 s. e.) is higher than the annual mean daytime UHI effect (2.1 K ±0.3 K). The daytime UHI effect is strongest in summer and weakest in winter but contrasts with the seasonal variation characteristics of nighttime UHI effect. During daytime, UHI effects in humid and semi-humid regions are much more obvious than those in semi-arid/arid regions; during nighttime, the UHI effect in semi-humid and semi-arid/arid regions is much stronger than that in humid regions. A Daytime Urban Cool Island effect exists in semi-arid/arid regions during spring, autumn, and winter seasons. Population, vegetation activity, and irrigation are three factors controlling annual mean daytime UHI effect. The nighttime UHI is significantly influenced by latitude, albedo, precipitation, and aerosol concentrations. We provide evidence for a long-held hypothesis that the biogeochemical effect of urban aerosols is an important contributor to the UHI effect. The important role played by rural background environment in calculating the UHI effect is further discussed in terms of surface aerodynamic roughness and the contrast in albedo between urban and rural areas. Mitigation of haze pollution has a co-benefit of reducing the UHI effect and heat stress for urban dwellers. It is also conducive to reducing negative impacts of regional and global climate change.

Key words: urban heat island (UHI); climate zone; aerosols; land surface temperature; remote sensing

城市气温或地表温度比周边乡村地区要高的现象称为城市热岛<sup>[1]</sup>.城市热岛强度可表征为城乡气温或地表温度的差异.目前超过全球50%的人口居住在城市地区,并持续增长<sup>[2]</sup>.在气候变暖背景下,城市热岛和天气事件,例如高温热浪协同作用<sup>[3]</sup>可改变局地能量交换甚至区域气候,对城市生态环境、人类健康和生存发展都带来极大威胁与挑战.

有研究表明,城市化进程所引起的下垫面生物物理学属性的改变:低反照率、低植被覆盖率、低蒸散量<sup>[4,5]</sup>以及大量人为热排放<sup>[5]</sup>,是造成城市热

收稿日期: 2017-02-21; 修订日期: 2017-05-03

基金项目: 国家自然科学基金项目(41575147); 江苏省高校优势学科建设工程项目(PAPD); 教育部长江学者和创新团队发展计划项目(PCSIRT); 江苏省2012年度普通高校研究生科研创新计划项目(CXLX12\_0502)

**作者简介:** 曹畅(1989~), 女, 博士研究生, 主要研究方向为地气交换, E-mail; ichangnj@ sina. com

岛现象产生的主要原因. 已有很多研究从城市形态 结构、经济发展状况、气象条件以及生物物理学因 子(反照率、蒸发)等方面探讨了城市热岛强度变化 及原因. 在城市形态结构上, 城市建筑物降低街区 天穹可见度, 使白天进入城市冠层的短波辐射通过 多次反射使城市冠层内部存储更多热量, 夜间则不 利于长波辐射散热[6]. 从城市规模、经济发展上, 不少研究者将人口或夜间灯光数据作为城市化发展 程度的标志, 发现其与城市热岛强度呈现显著正相 关关系[7,8]. 气象条件对城市热岛的影响体现在例 如:年平均降水量越多的地区其白天城市热岛强度 越高[7]; 夏季高压系统抑制边界层发展, 有利于城 市热岛现象产生[9]. 此外, 关于生物物理学因子的 研究表明城市低反照率[5]、低蒸散量[5]会加剧白天 城市热岛强度, 夜间城市建筑物和空调系统热排 放[5,6]会增强夜间城市热岛强度.

然而从生物化学角度探讨城市热岛现象的研究还不多见<sup>[5,7,10~12]</sup>. 近年来我国雾-霾污染严重,大气气溶胶颗粒能够通过散射、吸收等方式改变辐射交换从而影响城市能量平衡,进一步对城市热岛产生影响. 气溶胶对辐射的影响具有双重作用,一方面能有效散射人射太阳短波辐射造成进入城市冠层的短波辐射减少,另一方面在大气透明窗波段(8~12 μm)能有效散射地表发射的长波辐射<sup>[13]</sup>导致一部分长波辐射截留在城市冠层内部,这种双重作用对于白天和夜间城市热岛的影响机制亟待研究.

本研究的另一个科学动机是从区域气候背景探讨城市热岛的变化特征和形成机制.之前已有不少城市开展了城市热岛研究<sup>[14~16]</sup>,城市热岛强度的变化规律及其主控因子具有多样性<sup>[7,8,10]</sup>.从日变化上看,早期研究指出气温城市热岛是"夜间现象"即夜间呈现高峰<sup>[17]</sup>,但之后很多研究表明有些地区白天地表城市热岛强度突出<sup>[18]</sup>甚至超过夜间地表城市热岛强度<sup>[19]</sup>.从主控因子上看,城乡潜热蒸发的差异往往被认为是城市热岛强度的主控因子<sup>[5]</sup>,但是也有研究指出,城乡之间粗糙度不同导致的感热交换效率的差异才是主导因素<sup>[7]</sup>.但综合分析我国不同气候区城市热岛时空格局及成因的研究仍比较匮乏.

本研究选取我国 39 个城市并基于遥感卫星观测得到的地表温度数据(2003~2013年),明确我国城市热岛强度的空间变化特征,探讨生物物理学因子如白空反照率(white sky albedo, WSA)、归一化植被指数(normalized difference vegetation index,

NDVI)、生物化学因子如气溶胶光学厚度(aerosol optical depth, AOD)以及气象和人口等因子的影响. 验证雾-霾污染会加剧中国夜间城市热岛强度的科学假设,明确各因子对城市热岛的影响,以期为制定缓解中国城市热岛的政策措施提供可靠理论依据.

#### 1 材料与方法

### 1.1 站点选取

本研究选取中国大陆地区39个城市,选择标 准为每个省份至少选取1个城市,对于面积较大的 3个省份:内蒙古、新疆和青海、则额外选取2~3 个城市. 城市分布情况如图 1 所示. 根据 Zhao 等[7] 城乡像元选取方法,本研究中城市及周边乡村像元 点的选取依据 Moderate resolution imaging spectroradiometer (MODIS)卫星地表分类产品 MCD12Q1 中的 IGBP 分类, 并结合以下几点考量. 首先,确定城市像元点后,在其东南西北四个方位 分别选取合适乡村像元点. 其次, 城市像元点和乡 村像元点的纬度差异不超过0.1°,海拔高度差异不 大于100 m, 以此减少由于纬度或者海拔高度差异 造成的城乡温差. 最后, 所有选取的像元点在 Google Earth 中进行验证,以确保选取的准确性. 图 2 所示为 Google Earth 中长春[图 2(a)]和和田[图 2(b)]两座城市的城乡像元具体情况,其中红色圆 圈表示选取的像元. 从中可发现, 在两个城市东南 西北四个方位均存在满足上述条件的乡村像元. 此 外,长春和和田这两个城市在本研究中具有较好的

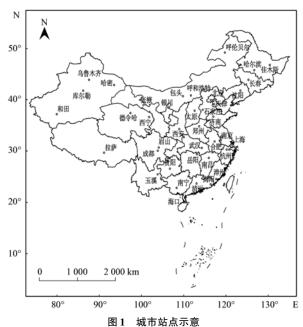


Fig. 1 Locations of the 39 cities selected in this study

代表性:首先两者处于不同气候区(表1),其次两者的乡村下垫面状况存在明显差异(图2). 长春市乡村像元点以农田生态系统为主,所占比例高达99%,而和田市乡村像元中农田所占比例仅为12%,荒漠占主要比例. 这种区域性乡村背景环境差异定会对城市热岛产生影响<sup>[7]</sup>. 研究中共有26

个城市由 3×3 个像元点组成,其余的城市只能选取 1~4 个纯城市像元点,这些像元点都位于选取城市的中心城区. 共有 18 个城市相对应的乡村像元位于城市像元东南西北四个方向. 基于 IGBP 分类标准,所有自然植被类型均作为乡村下垫面类型,水体像元点排除在外.





图 2 长春和和田城乡像元选取示意

Fig. 2 Urban and rural areas of Changchun and Hotan

城市热岛的研究对象是城市和其相应乡村地 区, 因此准确选取具有代表性的城市和乡村站点至 关重要. 本研究除了避免上文所提及的在选取城乡 像元点时会造成误差的方面,还考虑了研究期间地 表类型的动态变化并采取以下办法进行评估. 首 先, 选取 2010 年 MCD12Q1 数据作为初始选取城 市、乡村像元点的依据,由于城市像元点是中心城 区, 因此在2003~2010年之间由乡村转变为城市 的可能性很低. 另一方面, 城市化进程一般是不可 逆的, 因此 2010 年的乡村像元点是由城市像元点 转变而来的可能性也极低. 所以只需要再利用 2010 年之后的地表类型数据进行进一步验证即可, 这里 选取了2013年. 结果显示, 只有8个城市的乡村像 元点在2010~2013年间发生了城市化现象但程度 很轻: < 0.5% 的乡村像元点在 2013 年转变成了城 市像元点. 综上, 本研究所选取的城市和郊区像元 点具备充分的代表性.

#### 1.2 数据概况

研究所采用的是 2003 ~ 2013 年 MODIS 地表温度产品 MYD11A2,该产品依据分裂窗算法(splitwindow algorithm)计算得出晴空条件下的地表温度,时间分辨率为8d,空间分辨率为1km.由于雾-霾对遥感反演地表温度存在不确定性影响,在使用该产品前,笔者通过文献调研进行了准确性评估.

Wang 等<sup>[20]</sup>在美国 6 个地面辐射观测站研究发现,MODIS 地表温度产品与实际地面观测得出的地表温度差异为 -0.15 K  $\pm 0.73$  K(平均值  $\pm 1$  倍标准差,样本数 =6). 我国黑河地区的研究结果显示两者差异为 -0.17 K  $\pm 1.66$  K(同上,样本数 =4)<sup>[21]</sup>. 美国相对于我国,属于雾-霾程度较轻的清洁地区,但这两个地区 MODIS 反演地表温度和实际观测结果的差异并不显著(P=0.98),因此笔者认为该产品计算结果基本不受雾-霾条件影响.

气溶胶光学厚度(AOD)数据来自 MODIS 二级产品 MYDO4\_3K, 其空间分辨率为 3 km, 相比 10 km 空间分辨率的气溶胶产品, 更适用于本研究的空间尺度. 气溶胶光学厚度(AOD)是表征气溶胶颗粒通过散射、吸收等作用对辐射削弱程度的指标(http://daac. gsfc. nasa. gov/PIP/shtml/aerosol \_ optical \_ thickness\_or\_depth. shtml), AOD 越高表示气溶胶的辐射削弱作用越强, 大气污染越严重. 在本研究中将AOD 用于指示气溶胶浓度. 植被指数 NDVI 和白空反照率 WSA 则分别来源于 MYD13Q1 和 MCD43A1.

2003~2013年的降水量和气温数据通过国家 气候中心网站(http://ncc. cma. gov. cn/Website/ index. php? ChannelID = 43&WCHID = 5)获取. 同 时期的人口数据根据《中国城市统计年鉴》查询得 到. 采用城市年平均人口作为人口统计指标.

表 1 选取城市和乡村像元点信息

Table 1 Information on the urban and rural areas

序号	省份	城市	城市	市像元		乡村像元
<b>戶</b>	省份	<b></b>	像元数	经度(E)/(°)	像元数	农田像元比例/%
1	北京	北京	9	116. 40	36	82
2	天津	天津	9	117. 16	20	87
3	上海	上海	9	121. 46	36	50
4	江苏	南京	9	118. 77	36	93
5	浙江	杭州	9	120. 16	20	54
6	湖北	武汉	9	114. 27	18	100
7	河南	郑州	9	113. 65	27	100
8	安徽	合肥	9	117. 28	36	97
9	山东	济南	9	116. 98	36	99
10	河北	石家庄	9	114. 48	20	90
11	山西	太原	9	112. 57	18	62
12	辽宁	沈阳	9	123. 43	28	92
13	黑龙江	哈尔滨	9	126. 67	36	100
14	吉林	长春	9	125. 31	36	99
15	陕西	西安	9	108. 94	36	99
16	海南	海口	9	110. 35	12	36
17	贵州	贵阳	9	106. 71	36	
18	内蒙古	呼和浩特	9	111. 69	18	30
19	内蒙古	包头	V 9	109. 82	19	/2
20	广西	南宁	9	108. 32	27	21
21	湖南	岳阳	A 9	113. 13	18	72
22	新疆	乌鲁木齐	(9)	87. 56	18	-F0 (3 5
23	新疆	哈密	64/9	93. 51	27	16
24	新疆	库尔勒	3	86. 16	27	7
25	《 / / 四川	成都	9	104. 07	18	50
26	四川	眉山 //	2	103. 83	27	28
27	广东	揭阳	3	116. 37	3	0
28	/ / 江西	南昌	/ ( 4 / \	115. 91	12	100
29	青海	西宁	1 13/M	101. 80	3	33
30	云南	玉溪	4	103. 80	3	25
31/	宁夏	银川	4	106. 27	27	20
32	甘肃	张掖	2	100. 46	11	15
33	西藏	拉萨	3	91. 13	4	50
34	福建	漳州	9	117. 67	18	0
35	黑龙江	佳木斯	9	130. 36	18	100
36	内蒙古	呼伦贝尔	2	119. 73	3	0
37	青海	德令哈	1	97. 36	3	0
38	新疆	和田	2	79. 92	36	12
39	广东	清远	1	113. 03	3	67

#### 1.3 研究方法

2003~2013 年 MODIS 白天和夜间地表温度数据经计算整理成年平均值及四季多年平均值[春(3~5月)、夏(6~8月)、秋(9~11月)、冬(12~2月)]. 同期 WSA、NDVI 和 AOD 数据均先计算得到城市站点和其相应乡村站点差值(ΔWSA、ΔNDVI和 ΔAOD)然后得出多年以及四季平均值. 降水量、气温也经计算得到年平均和季节平均值. 人口数据为 2003~2013 年平均值. 农田像元比例为农田像

元点个数与乡村像元点总数的比值. 全国气溶胶背景浓度(图 8)是通过将 MYD04\_3K 提取得到的乡村气溶胶 AOD 值在 ArcGIS 10.2 中采用 Kriging 方法空间插值得到.

为便于考虑气候背景对城市热岛的影响,本研究采用 Köppen-Geiger 气候区划<sup>[22]</sup>,将所选取的 39个城市归类为湿润区(共19个城市)、半湿润区(共9个城市)和半干旱/干旱区(共11个城市). 具体分类情况如表 2 所示.

#### 表 2 湿润区、半湿润区和半干旱/干旱区城市分类

Table 2 List of cities that belong to humid, semi-humid, and semi-arid regions according to Köppen-Geiger climate classification

_	
气候区类型	城市
48に25主	With the state of
湿润区	上海、南京、杭州、武汉、郑州、合肥、济南、西安、海口、贵阳、南宁、岳阳、成都、眉山、揭阳、南昌、玉溪、漳州、清远
DE 11-4 E.S.	工商、南水、加州、西风、州州、日旭、州州、日文、西口、州州、州门、田阳、州州、周田、周阳、南田、王庆、泽州、田及
半湿润区	北京、天津、石家庄、太原、沈阳、哈尔滨、长春、佳木斯、呼伦贝尔
半干旱/干旱区	呼和浩特、包头、乌鲁木齐、哈密、库尔勒、西宁、银川、张掖、拉萨、哈令德、和田

### 2 结果与分析

#### 2.1 中国城市热岛时空变化

#### 2.1.1 中国不同气候区城市热岛昼夜变化

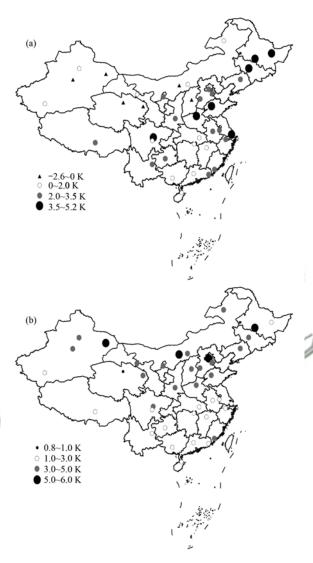
图 3 为 2003 ~ 2013 年白天和夜间城市热岛强度的空间变化. 我国不同气候区城市热岛强度存在明显差异. 在白天,湿润区(2.8 K±0.3 K,平均值±1 倍标准误差,下文同此)、半湿润区(2.8 K±0.6 K)城市热岛强度明显高于半干旱/干旱区(0.1 K±0.5 K). 所有城市中位于湿润区的济南城市热岛强度最高,为 5.2 K. 郑州、成都、哈尔滨、上海、佳木斯和长春的热岛强度均高于 4 K. 德令哈市、包头、西宁、太原、库尔勒和哈密城市热岛强度为负值,其中德令哈市最低,为 -2.6 K,出现城市冷岛现象.

在夜间,湿润区城市热岛强度(2.8 K±0.2 K) 明显低于半湿润(4.3 K±0.3 K)和半干旱/干旱地区[3.5 K±0.4 K,图2(b)].夜间城市热岛强度最高值出现在半湿润区的哈尔滨(5.6 K).包头、北京和哈密城市热岛强度紧随其后,都高于5 K.最低值出现在德令哈市,仅为 0.8 K.夜间没有出现城市冷岛现象.

 $2003 \sim 2013$  年我国 39 个城市平均夜间城市热岛强度(3.4 K±0.2 K) 明显高于白天城市热岛强度(2.1 K±0.3 K, P < 0.001). 这一现象尤其在半干旱/干旱地区更为明显,该地区夜间城市热岛强度为 3.5 K±0.4 K, 而白天热岛强度仅为 0.1 K±0.5 K.

### 2.1.2 中国不同气候区城市热岛季节变化

我国不同气候区城市热岛的季节变化与年平均趋势基本一致(图4).除夏季以外,湿润区白天城市热岛强度在其他3个季节均为最高.值得注意的是在春、秋、冬三季,半干旱/干旱区均出现白天城市冷岛现象,其中春季(-0.8 K±0.6 K)比秋季(-0.7 K±0.4 K)和冬季(-0.6 K±0.7 K)更强.湿润区夜间城市热岛强度在一年四季均低于半湿润区和半干旱/干旱区.在春、秋、冬三季,半湿润区夜间城市热岛强度均为最高.



(a) 年平均白天城市热岛强度空间变化;

(b)年平均夜间城市热岛强度空间变化

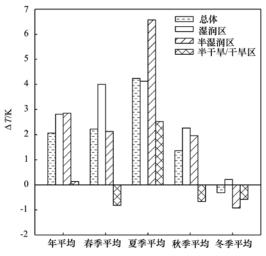
图 3 2003~2013年中国城市热岛白天和夜间空间变化

Fig. 3 Daytime and nighttime spatial variations in surface UHI effect for 39 cities in mainland China during 2003-2013

从昼夜对比上看,白天城市热岛强度呈现夏季  $(3.4 \text{ K} \pm 0.2 \text{ K})$ 高、冬季 $(-0.3 \text{ K} \pm 0.3 \text{ K})$ 低的现象.夜间城市热岛强度正好呈现相反的变化趋势,冬季 $(3.9 \text{ K} \pm 0.3 \text{ K})$ 最高而夏季 $(2.7 \text{ K} \pm 0.2 \text{ K})$ 最低.

## 2.2 城市热岛及其影响因子的关系

从图 5 白天城市热岛强度与各影响因子的相关



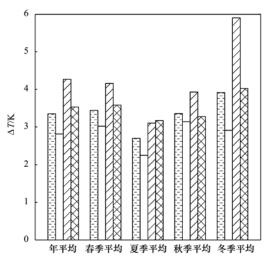


图 4 2003~2013年湿润区、半湿润区和半干旱/干旱区白天、夜间以及四季城市热岛强度

Fig. 4 Daytime, nighttime, and seasonal variation in surface UHI effect for three climate regions in mainland China during 2003-2013

性结果中可看出,影响年平均白天城市热岛强度 ( $\Delta T$ ) 主要有 3 个因子: 人口 ( $R^2$  = 0.47, P < 0.001)、农田像元比例( $R^2$  = 0.29, P < 0.001)和城 乡归一化植被指数差异  $\Delta NDVI$  ( $R^2$  = 0.31, P < 0.001).前两个因子与  $\Delta T$  存在明显的正相关关系, $\Delta NDVI$  则与  $\Delta T$  呈现显著负相关性。当去除农田像元比例超过 50%的站点后,年平均降水量与白天城市热岛强度也呈现显著的相关性(图 6).从季节上看,人口也是影响春、夏、秋三季  $\Delta T$  的主要因子(P < 0.001),农田像元比例与春、夏季  $\Delta T$  存在极强的正相关性(P < 0.001).  $\Delta NDVI$  只在秋季

与 $\Delta T$ 相关性很高,其余季节并没有呈现显著相关.

和白天不同,我国夜间城市热岛强度 ( $\Delta T$ ) 的主要控制因子为纬度 ( $R^2$  = 0.25,P < 0.01)、城乡反照率差异 ( $\Delta WSA$ ,  $R^2$  = 0.23,P < 0.01)、城乡气溶胶浓度差异 ( $\Delta AOD$ ,  $R^2$  = 0.18, P < 0.01)以及降水量 ( $R^2$  = 0.18, P < 0.01). 其中,降水量、 $\Delta WSA$ 分别与  $\Delta T$  呈现负相关关系,春、夏、冬三季  $\Delta T$  与纬度之间呈现显著正相关关系,夏、秋、冬三季  $\Delta T$  与  $\Delta WSA$  呈现明显负相关关系,春、夏季  $\Delta T$  与  $\Delta AOD$  存在显著正相关性.

图 7 所示为我国不同气候区年平均和四季城市

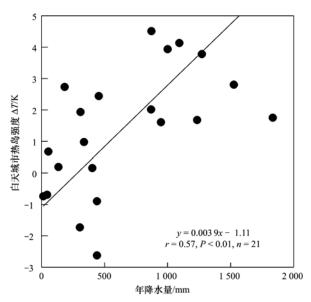
	年平均白天 UHI	春季白天 UHI	夏季白天 UHI	秋季白天 UHI	冬季白天 UHI	年平均夜间 UHI	春季夜间 UHI	夏季夜间 UHI	秋季夜间 UHI	冬季夜间 UHI
纬度	0.02	0.08	0.03	0.18**	0.03	0.25**	0.20**	0.21**	0.10	0.33***
降水量	0.09	0.09	0.02	0.22**	0.07	0.18**	0.19**	0.21**	0.03	0.25**
气温	0.05	0.08	0.00	0.28***	0.03	0.10	0.05	0.00	0.01	0.26***
$\Delta NDVI$	0.31***	0.05	0.02	0.43***	0.03	0.03	0.10*	0.06	0.00	0.03
农田像元比例	0.29***	0.30***	0.40***	0.10	0.16*	0.03	0.06	0.00	0.07	0.02
人口	0.47***	0.39***	0.31***	0.49***	0.00	0.05	0.06	0.01	0.12*	0.05
$\Delta$ WSA	0.00	0.30***	0.07	0.02	0.00	0.23**	0.02	0.31***	0.17*	0.40***
$\Delta AOD$	0.02	0.07	0.01	0.00	0.06	0.18**	0.13*	0.24**	0.02	0.06

灰色填充代表两者相关性为负相关,白色代表为正相关; \*\*\*代表显著性P<0.001,

\*\*代表显著性P < 0.01, \*代表显著性P < 0.05, 无\*表示相关性不显著

图 5 2003~2013年中国城市热岛强度与影响因子的相关性统计结果

Fig. 5 Correlations between the surface UHI effect in mainland China and eight impact factors during 2003-2013



去除农田像元比例超过50%站点

#### 图 6 白天城市热岛强度与年降水量关系

Fig. 6 Relationship between annual mean daytime surface

UHI effect and annual mean precipitation

热岛与各影响因子的相关性结果. 湿润区年平均白 天城市热岛强度受纬度、降水量、气温以及反照率 的影响[图 7(a)]. 除与纬度呈现正相关性以外, 与其他3个因子均呈现负相关性. 在湿润区内, 纬 度越高的城市年平均白天城市热岛强度越强. 降水 量和气温越高的城市, 年平均白天城市热岛强度反 而越低. 从季节上看, 春、夏季白天城市热岛强度 与降水量呈现显著负相关关系并和纬度呈现正相关 关系. 秋、冬季白天城市热岛强度受植被影响较大 (ΔNDVI、农田像元比例). 此外, 仅冬季白天城市热 岛强度与城乡气溶胶浓度差异呈现显著正相关性  $(\Delta AOD, R^2 = 0.46, P < 0.01)$ . 在此推测, 其主要原 因是冬季入射太阳短波辐射减少, 气溶胶对短波辐 射的削弱作用不如对向下长波辐射增强作用明显, 由此造成气溶胶浓度更高的城市地区接收更多的向 下长波辐射量,导致城市热岛效应增强.其他季节尤 其是太阳高度角较高的夏季, 气溶胶在白天对短波 和长波辐射的双重效应导致气溶胶对城市热岛的影 响不明显. 湿润区年平均夜间城市热岛强度仅与城 乡反照率差异(ΔWSA)呈现显著负相关性. 四季夜间 城市热岛强度的影响因子均较少, 纬度、 $\Delta NDVI$  和 降水量分别与春季、夏季和冬季城市热岛有显著相 关性, 秋季城市热岛与各因子均没有显著相关性.

半湿润区年平均城市热岛强度仅与农田像元比例呈现较为显著的正相关性( $R^2 = 0.50$ , P < 0.05)[图 7(b)].农田像元比例也是影响夏季以及秋季

白天城市热岛强度的重要因子.农田像元比例越高,城市热岛强度越强.降水量和城乡反照率差异增大,夏季白天城市热岛强度也相应增强.植被活动( $\Delta$ NDVI)和人口是秋季白天城市热岛强度的影响因子.在半湿润区,春季和冬季白天城市热岛强度与各影响因子之间都没有明显的相关性.人口与半湿润区年平均夜间城市热岛强度显著相关( $R^2 = 0.46$ ,P < 0.05).即在半湿润区,人口越多的城市年平均夜间城市热岛强度越高.除人口因素以外,气温和纬度与秋季夜间城市热岛均有显著性关系.但春、夏、冬这3个季节夜间城市热岛强度与各影响因子之间没有显著相关性.

与湿润区情况不同,半干旱/干旱区年平均白天城市热岛与各影响因子之间均没有呈现显著的相关性[图7(c)].春季和秋季同样如此.夏季白天城市热岛强度主要受到农田像元比例的影响(R²=0.46,P<0.05).在半干旱/干旱区,水分是主要的气象限制因子.农田灌溉造成乡村地区潜热蒸发增强,从而导致白天城市热岛效应增强.冬季白天城市热岛的影响因子是降水量,并呈现正相关关系(R²=0.64,P<0.01).这与湿润区情况相反.在半干旱/干旱地区,人口和城乡气溶胶浓度(ΔΑΟD)差异越大,夜间年平均城市热岛强度越高.人口也是影响春、夏、冬三季夜间城市热岛强度的主要因子.夏季夜间城市热岛强度还受到反照率和气溶胶浓度的影响.

#### 3 讨论

## 3.1 我国城市热岛现象主要控制因子分析

上述结果表明,我国白天城市热岛与人口、植被、农田比例相关性很高.城市人口通常可作为城市化发展程度或者城市扩张的标志,人口越多代表城市化发展程度越高.植被蒸发能够影响城市热岛[7].城市地区不透水面积相对较多,导致植被覆盖率比乡村低,城乡之间植被覆盖率差异可用  $\Delta$ NDVI 近似表示,通常为负值.本研究结果显示,城乡 NDVI 差异越大白天城市热岛强度越强,表明城乡地区通过植被蒸发降温的差异也越大,进一步加剧白天城市热岛强度.以往研究结果显示, $\Delta$ NDVI 与  $\Delta$ T 在夏季即植被生长季存在很强负相关性[11],而本研究中则是在秋季两者负相关性高.此外,Zhao 等[7]的研究结果发现,在北美地区年降水量和白天城市热岛强度呈现显著正相关性(P < 0.001),本研究中两者相关性很弱(P = 0.06).笔

(a)	年平均白天 UHI	春季白天 UHI	夏季白天 UHI	秋季白天 UHI	冬季白天 UHI	年平均夜间 UHI	春季夜间 UHI	夏季夜间 UHI	秋季夜间 UHI	冬季夜间 UHI	
纬度	0.28*	0.61***	0.50***	0.16	0.35*	0.10	0.28*	0.09	0.12	0.00	
降水量	0.38**	0.25*	0.41**	0.05	0.01	0.19	0.19	0.19	0.03	0.24*	
气温	0.26*	0.37**	0.18	0.13	0.26*	0.07	0.17	0.00	0.07	0.00	
ΔNDVI	0.00	0.00	0.05	0.01	0.40**	0.10	0.07	0.43**	0.01	0.06	
农田像元比例	0.00	0.19	0.10	0.40**	0.60***	0.04	0.10	0.08	0.09	0.01	
人口	0.20	0.29*	0.17	0.01	0.09	0.02	0.07	0.01	0.05	0.00	
$\Delta WSA$	0.29*	0.00	0.04	0.06	0.02	0.26*	0.07	0.22	0.20	0.14	
$\Delta AOD$	0.01	0.00	0.03	0.09	0.46**	0.14	0.05	0.15	0.01	0.19	
(b)											
纬度	0.04	0.06	0.01	0.01	0.20	0.17	0.31	0.21	0.48*	0.00	
降水量	0.43	0.15	0.81**	0.09	0.14	0.09	0.05	0.20	0.27	0.00	
气温	0.00	0.01	0.14	0.13	0.19	0.19	0.33	0.23	0.52*	0.00	
ΔNDVI	0.10	0.19	0.00	0.67**	0.03	0.17	0.08	0.04	0.00	0.00	
农田像元比例	0.50*	0.12	0.83***	0.61*	0.16	0.13	0.14	0.15	0.13	0.07	1 10
人口	0.19	0.06	0.29	0.47*	0.30	0.46*	0.41	0.44	0.56*	0.25	-
$\Delta WSA$	0.15	0.02	0.46*	0.20	0.02	0.17	0.40	0.03	0.24	0.14	
$\Delta AOD$	0.28	0.05	0.06	0.13	0.00	0.18	0.17	0.02	0.00	0.08	
(c)											
纬度	0.06	0.26	0.17	0.10	0.20	0.33	0.19	0.36	0.33	0.39*	
降水量	0.00	0.00	0.06	0.04	0.64**	0.06	0.13	0.11	0.02	0.02	
气温	0.04	0.02	0.02	0.07	0.06	0.02	0.02	0.29	0.03	0.27	
ΔNDVI	0.08	0.02	0.20	0.17	0.32	0.00	0.28	0.14	0.00	0.00	
农田像元比例	0.20	0.23	0.46*	0.28	0.12	0.00	0.01	0.00	0.00	0.00	
人口	0.15	0.02	0.23	0.17	0.02	0.40*	0.41*	0.37*	0.29	0.48*	
$\Delta WSA$	0.02	0.07	0.15	0.10	0.27	0.20	0.07	0.45*	0.16	0.28	
$\Delta AOD$	0.03	0.00	0.04	0.15	0.01	0.46*	0.11	0.46*	0.15	0.05	

(a)湿润区;(b)半湿润区;(c)半干旱/干旱区;灰色填充代表两者相关性为负相关,白色代表为正相关; \*\*\*代表显著性 P<0.001,\*\*代表显著性 P<0.005,无\*表示相关性不显著

图 7 2003~2013年中国不同气候区城市热岛强度与影响因子的相关性统计结果

Fig. 7 Correlations between surface UHI of three climate zones in mainland China and eight impact factors during 2003-2013

者推测这与农田灌溉有很大关系. 我国农田占非城市下垫面类型的比例很高,这一点在选取乡村像元点时也得到了验证. 同时,我国约 48% 的农田除了接收雨水自然灌溉之外还接收额外人工灌溉<sup>[23]</sup>. 人工灌溉的农田生态系统在能量交换过程中与其他自然生态系统存在差异. 当去除农田像元比例超过50%的站点后,年降水量和白天城市热岛强度呈现显著的正相关性(图 6, R² = 0.32, P < 0.01).

我国夜间城市热岛的控制因子较多. 首先是纬 度, 夜间城市热岛的产生主要来源于储热释放以及 人为热排放. 地理纬度恰好是城市地区辐射平衡和 人为热排放的综合指示因子[24]. 城市之间纬度不 同导致白天吸收净辐射差异, 进而造成夜间储热释 放差异. 此外, 夏季和冬季城市地区的空调制冷以 及供暖所释放的人为热也会增强夜间城市热岛强 度. Wienert 等<sup>[24]</sup>通过对纬度范围跨越 43°S~65°N 的全球 223 个城市热岛强度最高值与纬度建立统计 关系发现, 两者之间呈现线性正相关关系. 本研究 结果也证实了这一现象,并且发现在冬季两者的正 相关性最为显著,这进一步表明辐射和人为热共同 作用对我国冬季夜间城市热岛强度的重要影响. 其 次,反照率也是关键因子. 它通过直接影响地表接 收的净辐射量,从而间接影响夜间储热释放量. 城 市中建筑物、道路等材料的反照率通常比自然植被 低,造成城乡之间的反照率差异为负值.加之城市 冠层内的短波辐射进行多次反射, 城市地区白天吸 收较多的净辐射, 而夜间向上长波辐射容易被截留 在城市冠层内部导致城市地区降温效率降低. 因 此, 低反照率和城市冠层效应共同作用导致夜间城 市热岛强度往往与城乡反照率差异呈现负相关 性[7,10,11]. 值得指出,本研究与前人研究结果不同 之处在于[7],人口不是夜间城市热岛强度的主控因 子, 气溶胶浓度对夜间城市热岛强度有显著影响. 这将在3.3节加以讨论.

与之前关于北美、欧洲一些国家的城市热岛研究结果不同<sup>[7,10,11,25]</sup>,我国城市热岛呈现夜间明显高于白天的特征.这与 Zhou 等<sup>[11]</sup>利用 MODIS 地表温度数据研究 2003~2011 年我国城市热岛昼夜变化的结果一致.只是本研究得到的城市热岛强度更强,这与选取的城市像元位于中心城区有关.

#### 3.2 乡村背景环境对城市热岛的影响

乡村背景环境对城市热岛的影响主要体现在两方面. 首先乡村的选取对计算城市热岛强度有直接影响. 其次在不同气候区中,乡村背景环境导致城

市热岛主控因子发生改变.

相比城市,乡村下垫面类型更为多样,因此选取具有代表性的乡村点是城市热岛研究中的关键问题.早期研究中,通常选取单一城市和其周边乡村进行定点观测,并没有过多关注乡村下垫面类型<sup>[8]</sup>,而且时间尺度较短,没有考虑乡村环境随时间转变的影响.但在时空尺度跨越较大的城市热岛研究中,合理的乡村下垫面选取方法显得尤为重要.这些方法包括通过夜间灯光数据划分城乡地区<sup>[26]</sup>,通过构建建筑密度分布图利用阈值划分城乡地区<sup>[11]</sup>等.基于前人研究的经验<sup>[11,27]</sup>,本研究中在选取乡村点时不仅考虑了地理因素的影响而且对乡村站点在研究时期内的动态发展做了评估,保证最终计算得出的城市热岛强度的准确性和代表性.

不同气候区之间,乡村背景环境不同导致城乡 生物物理学属性产生差异,从而导致不同气候区城 市热岛影响因子的作用有所不同. Cao 等[28] 研究发 现,城乡空气动力学粗糙度差异是我国湿润区和半 干旱/干旱区白天城市热岛强度的首要影响因子, 并且对这两个气候区白天城市热岛的贡献呈现相反 作用. 空气动力学粗糙度受下垫面类型影响很 大[29]. 美国东部森林地区空气动力学阻力为 39 s·m<sup>-1</sup>而西部低矮灌木区空气动力学阻力高达 66 s·m-1[7]. 空气动力学阻力越低, 粗糙度越大, 越有 利于感热交换[29]. 在我国半干旱/干旱区, 由于降 水量没有湿润区充沛,乡村地区出现森林植被的概 率很低,多数为低矮灌木、农田甚至为荒漠. 因此 和湿润区不同, 半干旱/干旱区城市粗糙度反而比 乡村地区高,造成城市的感热交换效率增强从而导 致白天城市地表温度低于乡村地表温度,即出现城 市冷岛现象. 位于美国西部半干旱/干旱地区的 Pheonix 城市[30]以及对北美干旱区的城市热岛研究 中均发现这一现象[7]. 其次, 乡村下垫面类型不同 还会引起城乡反照率差异. 我国半干旱/干旱地区 城乡反照率差异为 - 0.04, 而湿润地区为 - 0.01. Jin 等也曾指出[31], 乡村下垫面以农田、落叶林为 主的城市和以常绿针叶林为主的城市相比, 前者城 乡反照率差异更为明显. 城乡反照率差异对白天城 市热岛的影响程度虽然远不及粗糙度的影响, 但区 域性的差异非常显著[7,28]. 和半干旱/干旱区相反, 湿润区的城乡反照率差异甚至起到了缓解城市热岛 的作用[28].

#### 3.3 气溶胶对城市热岛的影响

作为雾-霾的主要成分, 大气气溶胶能有效影

响辐射交换<sup>[32]</sup>,引起大气环境生物化学属性的改变<sup>[33,34]</sup>.我国近些年雾-霾污染问题突出,城市作为人为排放气溶胶的主要来源,其生物化学属性对城市热岛的影响还未得到足够重视.

本研究中, 利用遥感 AOD 数据发现城乡气溶 胶浓度差异对夜间城市热岛强度有显著影响(图 5). 主要原因为气溶胶粒子在大气透明窗波段(8~ 12 μm) 具备很强的散射和吸收能力, 夜间城市地 表发射的长波辐射被气溶胶粒子散射,造成向下长 波辐射增加, 使得城市地表温度不能有效降低, 加 剧了夜间城乡地表温度差异. 这一现象在北京和其 乡村地区香河站点的长波辐射对比分析中得到了印 证[35]. 此外, 气溶胶粒径会影响其散射能力从而影 响对城市热岛的贡献. 笔者在先前的研究中[28], 通 过利用能量平衡方法估算了气溶胶对我国3个不同 气候区夜间城市热岛的贡献并发现在半干旱/干旱 区,雾-霾的影响最为突出可达0.7 K,而对湿润区 的影响仅为 0.05 K. 这是因为半干旱/干旱地区多 为粗颗粒气溶胶粒子, 其对长波辐射的散射能力更 强. 此外, 从图 5 中可发现, 气溶胶浓度对白天城 市热岛强度并没有显著贡献. 这与在白天情况下, 气溶胶颗粒对短波辐射和长波辐射有相反作用有 关. 在白天, 气溶胶颗粒在截留地表长波辐射增强 城市热岛强度的同时,还散射入射太阳短波辐射, 降低城市地区净辐射量,从而又在一定程度上减缓 了城市热岛效应. 研究表明, 这两种效应基本可以 互相抵消, 因此气溶胶对白天城市热岛效应的影响 很低[28]

此外,这一结果对于理解区域气候差异也有所 启示.如图 8 所示,如果将乡村作为背景场,我国

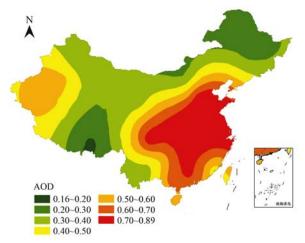


图 8 中国地区气溶胶光学厚度背景值

Fig. 8 Map of rural background aerosol optical depth (AOD) in China generated using an interpolation method

中东部和新疆部分地区是气溶胶分布的两个高值区. 平均气溶胶光学厚度为 0.55, 这比大气环境更为清洁的北美地区要高 0.39. 单独比较半干旱/干旱气候区, 我国比北美地区多接收 15 W·m<sup>-2</sup>的向下长波辐射<sup>[28]</sup>, 这对于我国夜间增温的影响不容小觑. 由此可见, 雾-霾治理能够起到缓解城市热岛效应, 减缓城市地区热胁迫的作用, 这必将对缓解区域甚至全球气候变化产生深远影响.

#### 4 结论

- (1)我国年平均夜间城市热岛强度(3.4 K±0.2 K)明显高于白天(2.1 K±0.3 K). 白天城市热岛强度呈现夏季高冬季低的变化规律,而夜间城市热岛强度的变化规律正好与之相反.
- (2)我国年平均城市热岛强度呈现明显的气候分区. 白天,湿润区和半湿润区明显高于半干旱/干旱区. 夜间,湿润区明显低于半湿润和半干旱/干旱区. 不同气候区城市热岛强度的季节性变化规律与年平均一致.
- (3)影响我国白天城市热岛强度的主要因子为 人口、农田灌溉和植被活动. 纬度、反照率、降水 量和气溶胶浓度是夜间城市热岛强度的主控因子.
- (4)乡村下垫面类型的不同在城乡粗糙度以及 反照率差异等方面对最终城市热岛效应的分析具有 重要影响.
- (5)雾-霾治理能够缓解我国夜间城市热岛效应,降低夜间增温速率,从而对于缓解区域甚至全球气候变化起到积极作用.

#### 参考文献:

- [ 1 ] Oke T R. The energetic basis of the urban heat island [ J ].
  Quarterly Journal of the Royal Meteorological Society, 1982, 108
  (455): 1-24.
- [2] World urbanization prospects; the 2014 Revision, (ST/ESA/SER. A/366)[R]. United Nations; Department of Economic and Social Affairs, Population Division, 2015.
- [3] Li D, Bou-Zeid E. Synergistic interactions between urban heat islands and heat waves; the impact in cities is larger than the sum of its parts[J]. Journal of Applied Meteorology and Climatology, 2013, 52(9): 2051-2064.
- [4] Voogt JA, Oke TR. Thermal remote sensing of urban climates [J]. Remote Sensing of Environment, 2013, 86(3): 370-384.
- [5] Taha H. Urban climates and heat islands; albedo, evapotranspiration, and anthropogenic heat [J]. Energy and Buildings, 1997, 25(2): 99-103.
- [6] Oleson K W, Bonan G B, Feddema J, et al. An urban parameterization for a global climate model. Part I: formulation and evaluation for two cities[J]. Journal of Applied Meteorology and Climatology, 2008, 47(4): 1038-1060.

- [7] Zhao L, Lee X, Smith R B, et al. Strong contributions of local background climate to urban heat islands [J]. Nature, 2014, 511 (7508): 216-219.
- [8] Oke T.R. City size and the urban heat island [J]. Atmospheric Environment, 1973, 7(8): 769-779.
- [ 9 ] Unwin D J. The synoptic climatology of Birmingham's urban heat island, 1965-74 [ J ]. Weather, 1980, 35(2): 43-50.
- [10] Peng S S, Piao S L, Ciais P, et al. Surface urban heat island across 419 global big cities [J]. Environmental Science & Technology, 2012, 46(2): 696-703.
- [11] Zhou D C, Zhao S Q, Liu S G, et al. Surface urban heat island in China's 32 major cities: spatial patterns and drivers [J]. Remote Sensing of Environment, 2014, 152: 51-61.
- [12] Wang J, Huang B, Fu D J, et al. Spatiotemporal variation in surface urban heat island intensity and associated determinants across major Chinese cities[J]. Remote Sensing, 2015, 7(4): 3670-3689.
- [13] Jacobson M Z. Studying the effects of aerosols on vertical photolysis rate coefficient and temperature profiles over an urban airshed[J]. Journal of Geophysical Research, 1998, 103 (D9): 10593-10604.
- [14] 彭保发, 石忆邵, 王贺封, 等. 城市热岛效应的影响机理及 其作用规律——以上海市为例[J]. 地理学报, 2013, 68 (11): 1461-1471. Peng B F, Shi Y S, Wang H F, et al. The impacting mechanism and laws of function of urban heat islands effect: a case study of Shanghai[J]. Acta Geographica Sinica, 2013, 68(11): 1461-1471.
- [15] Wang K, Wang J, Wang P, et al. Influences of urbanization on surface characteristics as derived from the Moderate-Resolution Imaging Spectroradiometer: a case study for the Beijing metropolitan area[J]. Journal of Geophysical Research, 2007, 112(D22): D22S06, doi: 10.1029/2006JD007997.
- [16] Meng F, Shan B Y, Liu M. Remote-sensing evaluation of the relationship between urban heat islands and urban biophysical descriptors in Jinan, China [J]. Journal of Applied Remote Sensing, 2014, 8(1): 083693.
- [17] Oke T R. Boundary layer climates (2nd ed.) [M]. London: Methuen & Co. Ltd, 1987. 435.
- [18] Tran H, Uchihama D, Ochi S, et al. Assessment with satellite data of the urban heat island effects in Asian mega cities [J].

  International Journal of Applied Earth Observation and Geoinformation, 2006, 8(1): 34-48.
- [19] Cheval S, Dumitrescu A. The July urban heat island of Bucharest as derived from MODIS images [J]. Theoretical and Applied Climatology, 2009, 96(1-2): 145-153.
- [20] Wang K C, Liang S L. Evaluation of ASTER and MODIS land surface temperature and emissivity products using long-term surface longwave radiation observations at SURFRAD sites [J]. Remote Sensing of Environment, 2009, 113 (7): 1556-

- 1565.
- [21] Yu W P, Ma M G, Wang X F, et al. Validation of MODIS land surface temperature products using ground measurements in the Heihe River Basin, China[A]. In: Proceedings of SPIE 8174, Remote Sensing for Agriculture, Ecosystems, and Hydrology X III [C]. Prague, Czech Republic: SPIE, 2011.
- [22] Rubel F, Kottek M. Observed and projected climate shifts 1901-2100 depicted by world maps of the Köppen-Geiger climate classification [J]. Meteorologische Zeitschrift, 2010, 19 (2): 135-141.
- [23] Hu B, Cai N, Xu L. China green development index report 2011
  [M]. Beijing: Beijing Normal University Press, 2011. 49-78.
- [24] Wienert U, Kuttler W. The dependence of the urban heat island intensity on latitude a statistical approach [J]. Meteorologische Zeitschrift, 2005, 14(5): 677-686.
- [25] Pongrácz R, Bartholy J, Dezsö Z. Application of remotely sensed thermal information to urban climatology of Central European cities[J]. Physics and Chemistry of the Earth, Parts A/B/C, 2010, 35(1-2): 95-99.
- [26] Gallo K, Adegoke J, Owen T W, et al. Satellite-based detection of global urban heat island temperature influence [J]. Journal of Geophysical Research, 2002, 107 (D24): ACL 16-1-ACL 16-6, doi: 10.1029/2002JD002588.
- [27] Zhao S Q, Zhou D C, Liu S G. Data concurrency is required for estimating urban heat island intensity [J]. Environmental Pollution, 2016, 208: 118-224.
- [28] Cao C, Lee X H, Liu S D, et al. Urban heat islands in China enhanced by haze pollution [J]. Nature Communications, 2016,
  7: 12509, doi: 10.1038/ncomms12509.
- [29] Garratt J R. The atmospheric boundary layer [M]. Cambridge: Cambridge University Press, 1992. 57.
- [30] Georgescu M, Moustaoui M, Mahalov A, et al. An alternative explanation of the semiarid urban area "oasis effect" [J]. Journal of Geophysical Research, 2011, 116 (D24): D24113, doi: 10.1029/2011JD016720.
- [31] Jin M L, Dickinson R E, Zhang D. The footprint of urban areas on global climate as characterized by MODIS [J]. Journal of Climate, 2005, 18(10): 1551-1565.
- [32] Folberth G A, Rumbold S T, Collins W J, et al. Global radiative forcing and megacities [J]. Urban Climate, 2014, 1: 4-19.
- [33] Crutzen P J. New directions: the growing urban heat and pollution "island" effect-impact on chemistry and climate [J]. Atmospheric Environment, 2004, 38(21): 3539-3540.
- [34] Grimm N B, Faeth S H, Golubiewski N E, et al. Global change and the ecology of cities [J]. Science, 2008, 319(5864): 756-760.
- [35] Wang L L, Gao Z Q, Miao S G, et al. Contrasting characteristics of the surface energy balance between the urban and rural areas of Beijing[J]. Advances in Atmospheric Sciences, 2015, 32(4): 505-514.

# **HUANJING KEXUE**

Environmental Science (monthly)

Vol. 38 No. 10 Oct. 15, 2017

## **CONTENTS**

Correlation Analysis of the Urban Heat Island Effect and Its Impact Factors in China	CAO Chang, LI Xu-hui, ZHANG Mi, et al. (3987)
Application of Satellite Remote Sensing in NO <sub>x</sub> Emission Control	
Control Models and Effect Evaluation of Air Pollution in Jing-Jin-Ji Urban Agglomeration	
Pollution Characteristics of Aerosol Number Concentration in Winter and Spring in a Northern Suburb of Nanjing	
Source Apportionment and Size Distribution of Aerosols at Lin'an Atmosphere Regional Background Station During Winter	
Seasonal Variations in Particle Size Distribution and Water-soluble Ion Composition of Atmospheric Particles in Chengdu	
Seasonal Variation and Source Apportionment of Water-Soluble Ions in PM <sub>2,5</sub> in Quanzhou City	
Chemical Characteristics and Sources of Heavy Metals in Fine Particles in Beijing in 2011-2012	
Pollution Assessment and Source Analysis of Metals in PM <sub>2,5</sub> in Haicang District, Xiamen City, China	
Characteristics and Health Risk Assessment of Metallic Elements in PM <sub>2.5</sub> Fraction of Road Dust	
Seasonal Variations in PM <sub>10</sub> and Associated Chemical Species in Jiuxian Mountain in Fujian Province	
Characteristics of C2-C6 Hydrocarbons During the Winter Air Pollution Period in Beijing Urban Area	
Analysis of Atmospheric Particulate Matter Pollution Characteristics by LIDAR in Beijing During Spring Festival, 2016	
Influence Factors and Sensitivity of Ozone Formation in Langfang in the Summer	
Impact of Human Activities on Water-Rock Interactions in Surface Water of Lijiang River	
Distinguishing the Properties and Sources of the Dissolved Organic Matter in Karst Reservoir Water During Winter Using Three-Dim	
Study in Wulixia Reservoir of Guangxi Province	
Analysis of Temporal and Spatial Variations in Trace Element Migration in Karst Critical Zone; An Example of Jiguan Cave, Henar	
Eutrophication and Characteristics of Cyanobacteria Bloom in the Summer in Guishi Reservoir	
Spatial and Temporal Distribution of Chlorophyll a and Its Relationship to Algae and Environmental Factors in Aha Reservoir	0
Spatio-temporal Variations in Phytoplankton Community in Shahe Reservoir, Tianmuhu, China	
Spatio-temporal Variations, Contamination and Potential Ecological Risk of Heavy Metals in the Sediments of Chenghai Lake	
Characteristics of Phosphorus Output Through Runoff on a Red Soil Slope Under Natural Rainfall Conditions	
Occurrence, Distribution and Health Risk of the Phthalate Esters in Riparian Soil in the Fluctuating Zone of the Three Gorges Rese	
occurrence, Distribution and Teath files of the Findance Listers in repartant con in the Findancing Zone of the Time Conges rese.	VANC Ting HF Ming-jing VANC 7hi-hao et al. (4187)
Seasonal Distribution, Composition, and Source Apportionment of Polycyclic Aromatic Hydrocarbons and Organochlorine Pesticides	
coasona Distributori, composition, and coase appointment of 1979/the Homate Hydrocarons and Organication Festivates	
Occurrence and Human Exposure Risk Assessment of Organophosphate Esters in Drinking Water in the Weifang Binhai Economic-T	
occurrence and remain Exposure risks researched to organisation properties and remain plantal resonance is	DONG Zheng MA Yu-long II lun-gi et al. (4212)
Contamination Characteristics and Human Exposure to Organophosphate Flame Retardants in Road Dust from Suzhou City	
Cancer Risk of Human Intake of PAH-Contaminated Particles Based on Hand-to-Mouth Activities	
Spatio-temporal Evolution of Groundwater Vulnerability Based on Spatial Autocorrelation	
Preparation of Ag-AgL/CN/MA Composites and Their Visible-light Photocatalytic Performance	
Effect of Eichhornia crassipes on Ammoxidation and Denitrification Microorganisms in Eutrophic Freshwaters	
	LI Jie, JIANG Li-juan, WANG Xiao-lin, et al. (4253)
Utilization of Copper ( II ) Wastewater for Enhancing the Treatment of Chromium ( VI) Wastewater in Microbial Fuel Cells	II Jie, JIANG Li-juan, WANG Xiao-lin, et al. (4253) XIONG Xiao-min, WU Xia-yuan, JIA Hong-hua, et al. (4262)
Utilization of Copper ( II ) Wastewater for Enhancing the Treatment of Chromium ( VI) Wastewater in Microbial Fuel Cells ······· Efficiency and Microecology of a Soil Infiltration System with High Hydraulic Loading for the Treatment of Swine Wastewater ·····	
Utilization of Copper ( II ) Wastewater for Enhancing the Treatment of Chromium ( VI ) Wastewater in Microbial Fuel Cells  Efficiency and Microecology of a Soil Infiltration System with High Hydraulic Loading for the Treatment of Swine Wastewater  Effects of Bacteria on the Growth of and Lipid Accumulation in Chlorella pyrenoidosa Cultivated in Municipal Wastewater	
Utilization of Copper ( II ) Wastewater for Enhancing the Treatment of Chromium ( VI ) Wastewater in Microbial Fuel Cells  Efficiency and Microecology of a Soil Infiltration System with High Hydraulic Loading for the Treatment of Swine Wastewater  Effects of Bacteria on the Growth of and Lipid Accumulation in Chlorella pyrenoidosa Cultivated in Municipal Wastewater  Enhanced Antibiotic Resistant Bacteria Removal from Wastewater Treatment Plant by Different Disinfection Technologies	
Utilization of Copper (II) Wastewater for Enhancing the Treatment of Chromium (VI) Wastewater in Microbial Fuel Cells  Efficiency and Microecology of a Soil Infiltration System with High Hydraulic Loading for the Treatment of Swine Wastewater  Effects of Bacteria on the Growth of and Lipid Accumulation in Chlorella pyrenoidosa Cultivated in Municipal Wastewater  Enhanced Antibiotic Resistant Bacteria Removal from Wastewater Treatment Plant by Different Disinfection Technologies  Coking Wastewater Treatment Efficiency and Comparison of Acute Toxicity Characteristics of the AnMBR-A-MBR and A²-MBR Pro	
Utilization of Copper (II) Wastewater for Enhancing the Treatment of Chromium (VI) Wastewater in Microbial Fuel Cells  Efficiency and Microecology of a Soil Infiltration System with High Hydraulic Loading for the Treatment of Swine Wastewater  Effects of Bacteria on the Growth of and Lipid Accumulation in Chlorella pyrenoidosa Cultivated in Municipal Wastewater  Enhanced Antibiotic Resistant Bacteria Removal from Wastewater Treatment Plant by Different Disinfection Technologies  Coking Wastewater Treatment Efficiency and Comparison of Acute Toxicity Characteristics of the AnMBR-A-MBR and A <sup>2</sup> -MBR Pro Stability of the CANON Process Based on Real-Time Control Technologies	
Utilization of Copper (II) Wastewater for Enhancing the Treatment of Chromium (VI) Wastewater in Microbial Fuel Cells  Efficiency and Microecology of a Soil Infiltration System with High Hydraulic Loading for the Treatment of Swine Wastewater  Effects of Bacteria on the Growth of and Lipid Accumulation in Chlorella pyrenoidosa Cultivated in Municipal Wastewater  Enhanced Antibiotic Resistant Bacteria Removal from Wastewater Treatment Plant by Different Disinfection Technologies  Coking Wastewater Treatment Efficiency and Comparison of Acute Toxicity Characteristics of the AnMBR-A-MBR and A <sup>2</sup> -MBR Pro Stability of the CANON Process Based on Real-Time Control Technologies  Improving Nitrogen and Phosphorus Removal from Reclaimed Water Using a Novel Sulfur/Iron Composite Filler	
Utilization of Copper (II) Wastewater for Enhancing the Treatment of Chromium (VI) Wastewater in Microbial Fuel Cells  Efficiency and Microecology of a Soil Infiltration System with High Hydraulic Loading for the Treatment of Swine Wastewater  Effects of Bacteria on the Growth of and Lipid Accumulation in Chlorella pyrenoidosa Cultivated in Municipal Wastewater  Enhanced Antibiotic Resistant Bacteria Removal from Wastewater Treatment Plant by Different Disinfection Technologies  Coking Wastewater Treatment Efficiency and Comparison of Acute Toxicity Characteristics of the AnMBR-A-MBR and A <sup>2</sup> -MBR Pro Stability of the CANON Process Based on Real-Time Control Technologies  Improving Nitrogen and Phosphorus Removal from Reclaimed Water Using a Novel Sulfur/Iron Composite Filler  Start-up and Capacity Enhancement of a Partial Nitrification Pilot Reactor in Continuous Flow	
Utilization of Copper ( II ) Wastewater for Enhancing the Treatment of Chromium ( VI ) Wastewater in Microbial Fuel Cells  Efficiency and Microecology of a Soil Infiltration System with High Hydraulic Loading for the Treatment of Swine Wastewater  Effects of Bacteria on the Growth of and Lipid Accumulation in Chlorella pyrenoidosa Cultivated in Municipal Wastewater  Enhanced Antibiotic Resistant Bacteria Removal from Wastewater Treatment Plant by Different Disinfection Technologies  Coking Wastewater Treatment Efficiency and Comparison of Acute Toxicity Characteristics of the AnMBR-A-MBR and A <sup>2</sup> -MBR Pro Stability of the CANON Process Based on Real-Time Control Technologies  Improving Nitrogen and Phosphorus Removal from Reclaimed Water Using a Novel Sulfur/Iron Composite Filler  Start-up and Capacity Enhancement of a Partial Nitrification Pilot Reactor in Continuous Flow  Quick Start-up Performance of Combined ANAMMOX Reactor Based on Different Inoculated Sludge Types	
Utilization of Copper (II) Wastewater for Enhancing the Treatment of Chromium (VI) Wastewater in Microbial Fuel Cells  Efficiency and Microecology of a Soil Infiltration System with High Hydraulic Loading for the Treatment of Swine Wastewater  Effects of Bacteria on the Growth of and Lipid Accumulation in Chlorella pyrenoidosa Cultivated in Municipal Wastewater  Enhanced Antibiotic Resistant Bacteria Removal from Wastewater Treatment Plant by Different Disinfection Technologies  Coking Wastewater Treatment Efficiency and Comparison of Acute Toxicity Characteristics of the AnMBR-A-MBR and A²-MBR Pro Stability of the CANON Process Based on Real-Time Control Technologies  Improving Nitrogen and Phosphorus Removal from Reclaimed Water Using a Novel Sulfur/Iron Composite Filler  Start-up and Capacity Enhancement of a Partial Nitrification Pilot Reactor in Continuous Flow  Quick Start-up Performance of Combined ANAMMOX Reactor Based on Different Inoculated Sludge Types  Effect of Two-Stage Aeration on Nitrogen Removal Performance of Aerobic Granular Sludge	
Utilization of Copper ( II ) Wastewater for Enhancing the Treatment of Chromium ( VI ) Wastewater in Microbial Fuel Cells  Efficiency and Microecology of a Soil Infiltration System with High Hydraulic Loading for the Treatment of Swine Wastewater  Effects of Bacteria on the Growth of and Lipid Accumulation in Chlorella pyrenoidosa Cultivated in Municipal Wastewater  Enhanced Antibiotic Resistant Bacteria Removal from Wastewater Treatment Plant by Different Disinfection Technologies  Coking Wastewater Treatment Efficiency and Comparison of Acute Toxicity Characteristics of the AnMBR-A-MBR and A²-MBR Pro Stability of the CANON Process Based on Real-Time Control Technologies  Improving Nitrogen and Phosphorus Removal from Reclaimed Water Using a Novel Sulfur/Iron Composite Filler  Start-up and Capacity Enhancement of a Partial Nitrification Pilot Reactor in Continuous Flow  Quick Start-up Performance of Combined ANAMMOX Reactor Based on Different Inoculated Sludge Types  Effect of Two-Stage Aeration on Nitrogen Removal Performance of Aerobic Granular Sludge  Construction of a High Efficiency Anaerobic Digestion System for Vinegar Residue	
Utilization of Copper (II) Wastewater for Enhancing the Treatment of Chromium (VI) Wastewater in Microbial Fuel Cells  Efficiency and Microecology of a Soil Infiltration System with High Hydraulic Loading for the Treatment of Swine Wastewater  Effects of Bacteria on the Growth of and Lipid Accumulation in Chlorella pyrenoidosa Cultivated in Municipal Wastewater  Enhanced Antibiotic Resistant Bacteria Removal from Wastewater Treatment Plant by Different Disinfection Technologies  Coking Wastewater Treatment Efficiency and Comparison of Acute Toxicity Characteristics of the AnMBR-A-MBR and A <sup>2</sup> -MBR Pro Stability of the CANON Process Based on Real-Time Control Technologies  Improving Nitrogen and Phosphorus Removal from Reclaimed Water Using a Novel Sulfur/Iron Composite Filler  Start-up and Capacity Enhancement of a Partial Nitrification Pilot Reactor in Continuous Flow  Quick Start-up Performance of Combined ANAMMOX Reactor Based on Different Inoculated Sludge Types  Effect of Two-Stage Aeration on Nitrogen Removal Performance of Aerobic Granular Sludge  Construction of a High Efficiency Anaerobic Digestion System for Vinegar Residue	
Utilization of Copper ( II ) Wastewater for Enhancing the Treatment of Chromium ( VI ) Wastewater in Microbial Fuel Cells  Efficiency and Microecology of a Soil Infiltration System with High Hydraulic Loading for the Treatment of Swine Wastewater  Effects of Bacteria on the Growth of and Lipid Accumulation in Chlorella pyrenoidosa Cultivated in Municipal Wastewater  Enhanced Antibiotic Resistant Bacteria Removal from Wastewater Treatment Plant by Different Disinfection Technologies  Coking Wastewater Treatment Efficiency and Comparison of Acute Toxicity Characteristics of the AnMBR-A-MBR and A²-MBR Pro Stability of the CANON Process Based on Real-Time Control Technologies  Improving Nitrogen and Phosphorus Removal from Reclaimed Water Using a Novel Sulfur/Iron Composite Filler  Start-up and Capacity Enhancement of a Partial Nitrification Pilot Reactor in Continuous Flow  Quick Start-up Performance of Combined ANAMMOX Reactor Based on Different Inoculated Sludge Types  Effect of Two-Stage Aeration on Nitrogen Removal Performance of Aerobic Granular Sludge  Construction of a High Efficiency Anaerobic Digestion System for Vinegar Residue	
Utilization of Copper ( II ) Wastewater for Enhancing the Treatment of Chromium ( VI ) Wastewater in Microbial Fuel Cells  Efficiency and Microecology of a Soil Infiltration System with High Hydraulic Loading for the Treatment of Swine Wastewater  Effects of Bacteria on the Growth of and Lipid Accumulation in Chlorella pyrenoidosa Cultivated in Municipal Wastewater  Enhanced Antibiotic Resistant Bacteria Removal from Wastewater Treatment Plant by Different Disinfection Technologies  Coking Wastewater Treatment Efficiency and Comparison of Acute Toxicity Characteristics of the AnMBR-A-MBR and A²-MBR Pro Stability of the CANON Process Based on Real-Time Control Technologies	
Utilization of Copper ( II ) Wastewater for Enhancing the Treatment of Chromium ( VI ) Wastewater in Microbial Fuel Cells  Efficiency and Microecology of a Soil Infiltration System with High Hydraulic Loading for the Treatment of Swine Wastewater  Effects of Bacteria on the Growth of and Lipid Accumulation in Chlorella pyrenoidosa Cultivated in Municipal Wastewater  Enhanced Antibiotic Resistant Bacteria Removal from Wastewater Treatment Plant by Different Disinfection Technologies  Coking Wastewater Treatment Efficiency and Comparison of Acute Toxicity Characteristics of the AnMBR-A-MBR and A²-MBR Pro Stability of the CANON Process Based on Real-Time Control Technologies  Improving Nitrogen and Phosphorus Removal from Reclaimed Water Using a Novel Sulfur/Iron Composite Filler  Start-up and Capacity Enhancement of a Partial Nitrification Pilot Reactor in Continuous Flow	
Utilization of Copper ( II ) Wastewater for Enhancing the Treatment of Chromium ( VI ) Wastewater in Microbial Fuel Cells	
Utilization of Copper ( II ) Wastewater for Enhancing the Treatment of Chromium ( VI ) Wastewater in Microbial Fuel Cells	
Utilization of Copper ( II ) Wastewater for Enhancing the Treatment of Chromium ( VI) Wastewater in Microbial Fuel Cells	
Utilization of Copper ( II ) Wastewater for Enhancing the Treatment of Chromium ( VI) Wastewater in Microbial Fuel Cells	
Utilization of Copper ( II ) Wastewater for Enhancing the Treatment of Chromium ( VI) Wastewater in Microbial Fuel Cells	
Utilization of Copper (II) Wastewater for Enhancing the Treatment of Chromium (VI) Wastewater in Microbial Fuel Cells	
Utilization of Copper ( II ) Wastewater for Enhancing the Treatment of Chromium ( VI) Wastewater in Microbial Fuel Cells	